Korean J. Electron Microscopy Special Issue 1, 47~56(2006)

Phase Identification of Nano-Phase Materials using Convergent Beam Electron Diffraction (CBED) Technique

Gyeungho Kim* and Jae-Pyoung Ahn
Nano-Materials Research Center, Korea Institute of Science and Technology,
P. O. Box 131, Cheongryang, Seoul 130-650, Korea
(Received April 11, 2005; Accepted March 24, 2006)

ABSTRACT

Improvements are made to existing primitive cell volume measurement method to provide a real-time analysis capability for the phase analysis of nanocrystalline materials. Simplification is introduced in the primitive cell volume calculation leading to fast and reliable method for nano-phase identification and is applied to the phase analysis of Mo-Si-N nanocoating layer. In addition, comparison is made between real-time and film measurements for their accuracy of calculated primitive cell volume values and factors governing the accuracy of the method are determined. About 5% accuracy in primitive cell determination is obtained from camera length calibration and this technique is used to investigate the cell volume variation in WC-TiC core-shell microstructure. In addition to chemical compositional variation in core-shell type structure, primitive cell volume variation reveals additional information on lattice coherency strain across the interface.

Key words : Convergent beam electron diffraction, Nanophase materials, Primitive cell volume

INTRODUCTION

Nano-phase materials draw considerable attention due to their unique properties ranging from various mechanical to physical properties such as optical, electrical and thermal characteristics (Pool, 2003). These materials include nanopowders, nanocomposites, semiconductor quantum dots and quantum well structures, nanowires and nanocoatings.

Characterization techniques of such materials require a nanoscale spatial resolution for crystal structure identification and chemical composition analysis. Convergent beam electron diffraction (CBED) technique in the transmission electron microscope (TEM) has been satisfactorily employed for nanoscale structural determination. However, practical application of CBED to nano-phase materials is hampered by several reasons. Firstly, reliable identification of phases requires several diffraction patterns with high symmetry from nano-grained phases and tilting the sample to several zone axes is quite difficult. Secondly, diffraction patterns from the nano-grain phases are indexed after recording the patterns to the film or CCD. This conventional process is tedious and more importantly, results of some constituent phases may be missing and/or redundant diffraction patterns are obtained from the same phases. Finally, size or thickness of the nano-grain phase does not allow dynamic diffraction and observation of higher order Laue zone (HOLZ) lines is often not possible.

Simple procedure of measuring and matching the primitive cell volume from a single CBED pattern in the TEM has distinct advantages in the phase identification of nano-phase materials (Page, 1992; Kim, 1996). This method is based on the fact that the volume of the primitive cell of a given phase is materials constant independent of a given zone axis. Furthermore, the combination of zero order Laue zone (ZOLZ) pattern which defines the projected area of the primitive cell and the HOLZ ring radius related to the height of the primitive

* Correspondence should be addressed to Dr. Gyeungho Kim, 39-1 Nano-materials Research Center, Korea Institute of Science and Technology, P. O. Box 131, Cheongryang, Seoul, 130-650, Korea. Ph.: (02) 958-5525, FAX: (02) 958-5529, E-mail: ghokim@kist.re.kr

cell is sufficient to provide a primitive cell volume of a given phase to about 10% accuracy. It should be emphasized that there is no need to obtain the HOLZ line pattern and even the spot pattern with small convergence angle at any low symmetry zone axis is acceptable. In fact, low symmetry zone axis pattern is preferred in this method since smaller HOLZ ring assures highly visible HOLZ spots and less prone to measurement errors. Improvements to be made in this technique are the real-time capability i.e., measuring of primitive cell volume from the CBED pattern during observation and better accuracy of the method. Real-time capability of primitive cell measurements allows confident phase identification of complex mixtures of nano-phases since primitive cell volume is measured from the region of interest before recording the pattern to the film and thus all possible phases in the sample can be discriminated and recorded in a single experiment. To facilitate the real-time pattern measurements of the primitive cell volume in a CBED pattern, simple equation for the calculation of primitive cell volume is necessary. However, simplification of the calculation should not deteriorate the accuracy of the method. Typical accuracy for primitive cell volume measurements using CBED is about 10% mainly determined by the error associated with camera length calibration and measurements of spot distances and angles. Careful calibration of camera length may improve the accuracy of the analysis to 5% or better and this improvement will expand the applicability of this technique to more critical evaluation of lattice parameter variations in nanoscale.

Simplified equations for real-time primitive cell volume measurements from observed CBED patterns will be derived in this study and examples will be given from Mo-Si-N system contains 3 intermetallic compounds and nano sized Si_3N_4 dispersants (Byun, 2002; Yoon, 2005). By comparing with film measurement results, the sources of error in real-time analysis technique will be identified and efforts will be devoted to improve the accuracy of primitive cell measurements. Possibility to investigate the structural variations in the core-shell type grains using primitive cell volume measurements will be explored in WC-TiC system.

MATERIALS AND METHODS

Mo-Si-N nanocoating specimen was prepared by a two-step metal organic chemical vapor deposition (MOCVD) method. Molybdenum metal plate was first siliconized by the deposition of Si performed in a gas mixture of $SiCl_4$ and H_2 at 1,100°C for 30 min to form $MoSi_2$ coating layer on Mo substrate. The flow rates of $SiCl_4$ and H_2 were fixed at 10 and 990 mL/min, respectively. $MoSi_2$ coating layer was then converted to Mo_5Si_3 phase by high temperature annealing treatment at 1,200°C for 70 hrs in H_2 atmosphere. Ammonia nitridation of a Mo_5Si_3 on Mo substrate was carried out at 1,100°C for 10 hrs. The purity and flow rate of NH_3 gas was 99.9999% and 100 mL/min, respectively. Finally, subsequent CVD of Si was performed at 1,100°C for 1 hr using the same deposition conditions. Upon completion of Si deposition, the power was turned off so that the sample was cooled to room temperature in H_2 gas stream.

Powders used to make (W, Ti)C-Co cermets were WC (average size of 1.36 μm, purity of 99.99% from H.C. Stark), Co (average size of 1.09 μm, purity of 99.9% from H.C. Stark), lamp black carbon from Fisher Scientific and TiC (average size of 1.02 μm, purity of 99.9% from H.C. Stark). WC-30wt% Co powder mixtures were milled in ethyl alcohol using WC balls for 24 hrs at a speed of 50~60 rpm. Drying of milled powder mixtures was done for 24 hrs at 10^{-1} torr. Dried powder mixtures were sieved, 2 wt% TiC powder was added and mixed by hand for 1 hr. Powder compacts were prepared by 12 mm diameter cylindrical mold with approximately one ton pressure. Sintering of the powder compacts was performed at 10^{-2} torr vacuum furnace at 1,500°C for 16 hrs with the heating rate of 10°C/min and forced cooling after sintering.

Cross sectional TEM sample from $MoSi_2$-Si_3N_4 coating sample was prepared by gluing the coating layer face-to-face with Gatan G1 epoxy and curing at 120°C for 1 hr. Glued sample was cut and polished to 100 μm in thickness. This sample was dimpled to 15 μm in final thickness by Gatan dimpler and ion milled in the Gatan Duomill operated at 6 kV, 0.5 mA Ar ion with specimen rocking and 15° of incident angle for both sides until perforation. Similar procedure was used to make TEM sample for (W, Ti)C-Co.

Microstructural observation and diffraction analysis of the samples was made by double tilting holder and Philips CM30 TEM operating at 200 kV. Camera length for diffraction pattern analysis in the TEM was calibra-

ted by using the silicon standard specimen. Calculation of primitive cell volume during observation and from the film was performed by the equations incorporated in Excel spreadsheet program.

RESULTS

1. Derivation of equations for real-time primitive cell volume measurements

Original equations for primitive cell volume measurements are given below.

$$A=\frac{L^2 \cdot \lambda^2}{R_1 \cdot R_2 \cdot \sin(ang)} \quad (1)$$

$$H^{-1}=\frac{\lambda}{1-\cos\left\{\tan^{-1}\left(\frac{CRAD}{L}\right)\right\}} \quad (2)$$

$$V=\frac{L^2 \cdot \lambda^2}{R_1 \cdot R_2 \cdot \sin(ang) \cdot \left[1-\cos\left\{\tan^{-1}\left(\frac{CRAD}{L}\right)\right\}\right]} \quad (3)$$

In the equations, R_1 and R_2 are ZOLZ spot distances measured from the pattern, ang is the angle between them, L is the camera length, λ is the electron wavelength and CRAD is the radius of HOLZ ring. Using 4 measured values (R_1, R_2, ang and CRAD) and two operating constants (L and λ), projected area, A in a given zone axis orientation and height along the beam direction, H^{-1} can be evaluated and the primitive cell volume is the product of these two quantities. In the real-time measurement, current through the beam deflection coil is manipulated to move the CBED pattern and the direction and magnitude of its translation can be displayed in nm units. Therefore, by moving the pattern on the screen, spot distances are automatically converted and displayed as interplanar spacing values from the relationship, $d=L\lambda/R$ or $DRAD=L\lambda/CRAD$. Equations for real-time measurements can be simplified as given below.

$$A_R=\frac{d_1 \cdot d_2}{\sin(ang)} \quad (4)$$

$$H_R^{-1}=\frac{2 \cdot DRAD^2}{\lambda} \quad (5)$$

$$V_R=\frac{2 \cdot d_1 \cdot d_2 \cdot DRAD^2}{\lambda \cdot \sin(ang)} \quad (6)$$

Similar to the original equations, A_R, H_R^{-1} and V_R indicates projected ZOLZ area, height perpendicular to the ZOLZ area and primitive cell volume calculated in real-time method, respectively. Major modification of equation is introduced in H_R^{-1} where Taylor series expansion of cosine term was employed to simplify the original equation. Results from two sets of equations are given in Fig. 1 taken from the standard silicon sample.

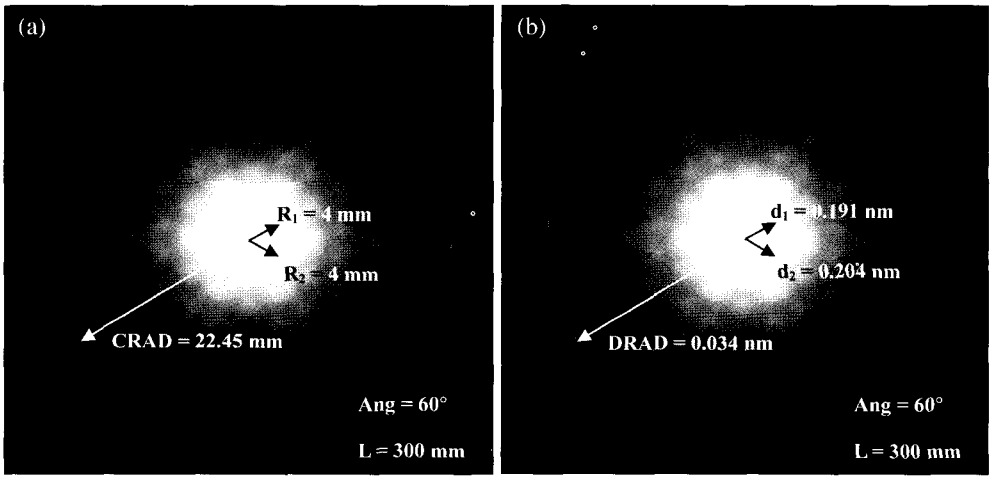

Fig. 1. Results of measurements for primitive cell volume calculation in (a) film measurement and (b) real-time measurement from the Si [111] CBED pattern.

Table 1. Estimation of errors in CBED pattern measurements

	Film measurements			Real-time measurements		
	ZOLZ	HOLZ	Primitive cell volume	ZOLZ	HOLZ	Primitive cell volume
Average error (%)	1.104	0.600	0.399	1.386	4.087	−2.853
Standard deviation (%)	2.008	4.353	4.372	0.995	4.252	3.035

Table 2. Results of phase analysis by primitive cell volume measurements of constituent phases in $MoSi_2$-Si_3N_4 nanocoating layer

Constituent phase	Theoretical primitive cell volume (Å^3)	Calculated values from film measurements (Å^3)	Calculated values from real-time measurements (Å^3)
Mo_3Si	109.07	113.14	114.55
Si_3N_4	296.24	284.77, 276.52	283.99, 306.40
Mo_2N	17.39	18.04	18.52
$MoSi_2$	38.12	39.60	39.68

2. Comparison of accuracy for primitive cell volume measurements

Errors in primitive cell volume measurements are evaluated by using several zone axis patterns from the *standard silicon sample. Using 8 different zone axis* patterns, total of 16 ZOLZ diffraction disc distances are measured and 8 HOLZ ring radii are measured in two methods. Table 1 summarizes results of error estimations in the pattern measurements. Overall error of two methods is comparable and up to 6% including the standard deviation. Largest error is found in the HOLZ radius measurement by real-time method and reaches up to 8%.

3. Phase identification in Mo-Si-N system

Table 2 lists constituent phases in $MoSi_2$-Si_3N_4 nanocoating layer along with their theoretical primitive cell volumes and the results of measurements by the two methods. Images of constituent phases and corresponding CBED patterns are given in Fig. 2.

4. Correction of errors in primitive cell volume measurements

There are two possible sources or errors in real-time measurements of primitive cell volume from CBED pattern. One is from the simplified equation for H_R^{-1} calculation and another is incorrect value of camera length. Standard CBED pattern of Si [001] orientation is used to evaluate the contributions from these two factors. Fig. 3 shows the Si [001] CBED pattern taken with small convergence angle. HOLZ ring radius is measured and measured value is used to calculate the H^{-1} and H_R^{-1} using Eq. (2) and Eq. (5), respectively. These calculated values are compared with theoretical value at [001] zone axis orientation. From the comparison, simplification of equation for real time measurement leads to only −0.7% deviation from the theoretical value and thus insignificant effect on the accuracy of the method. ZOLZ spot distances of (220), (400), (440), (800) and (660) are measured and converted to

$$r_{hkl} \cdot d_{hkl} = L \cdot \lambda \tag{7}$$

$$r_{hkl} \cdot d_{hkl} = L \cdot \lambda + \left(\frac{3}{8} \cdot \frac{\lambda}{L}\right) \cdot r_{hkl}^2 \tag{8}$$

$$r_{hkl} \cdot d_{hkl} = L \cdot \lambda + k \cdot r_{hkl}^2 \tag{9}$$

Eq. (7) was derived from simple geometrical linear relationship (Edington, 1976) and is constant of 7.4547 mm Å in this operating condition. Eq. (8) was introduced to correct for the curvature of the Ewald sphere (Andrews, 1971) and is $r_{hkl} \cdot d_{hkl} = 7.4547 + 3.17 \times 10^{-5} \cdot r_{hkl}^2$ in this case. Note that the correction term is constant. Finally, Eq. (9) was obtained from the least square fitting of measurements (Schamp, 2005) and was determined to be $r_{hkl} \cdot d_{hkl} = 7.375 + 1.09 \times 10^{-3} \cdot r_{hkl}^2$ from ZOLZ spots shown in Fig. 3. Comparison of three cases is given in Fig. 4 with measurement data from ZOLZ spots. Using the corrected values of three cases, average errors of primitive cell volume calculation are estimated and results are given in Table 3. It is found that typical value of primitive cell volume calculation from CBED pattern is less than 5% including the standard deviation of measurements.

5. Primitive cell volume measurements in WC-TiC core-shell structure

With 5% accuracy, it may be possible to apply this method to analyze the concentration gradient in the

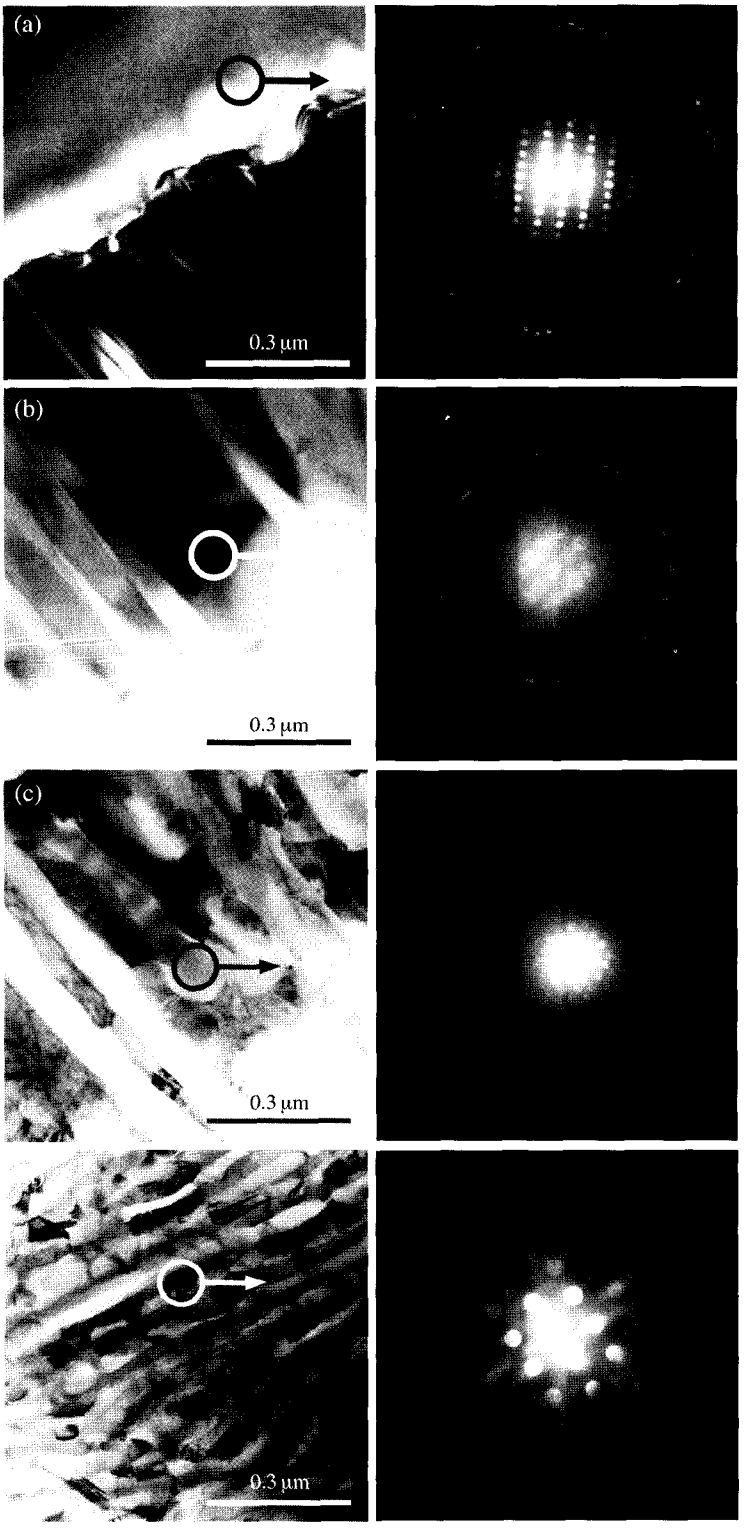

Fig. 2. TEM bright-field image of the constituent phases in Mo-Si-N system and corresponding CBED patterns obtained from the region marked by the circle and arrow, (a) Mo_3Si phase, (b) $MoSi_2$ phase, (c) Si_3N_4 phase and (d) Mo_2N phase.

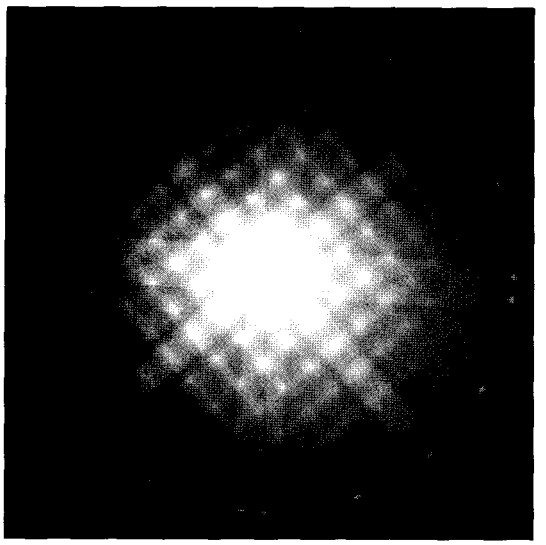

Fig. 3. [001] CBED pattern from the silicon showing ZOLZ discs and First order Laue zone (FOLZ) ring.

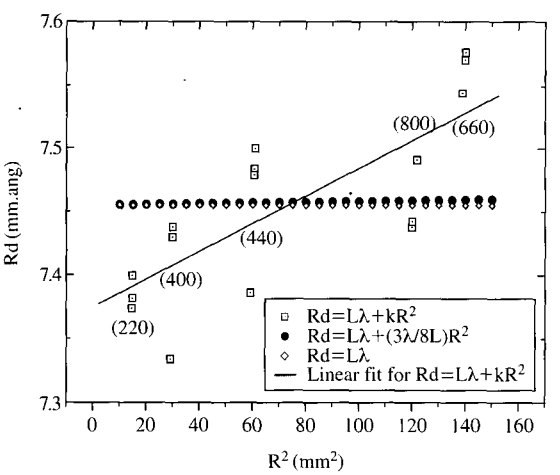

Fig. 4. Spot distances of ZOLZ spots from Si [001] pattern and their fitting curves from 3 models for camera length correction.

core-shell type microstructure. TiC-WC grain has a typical core-shell morphology and TiC, WC and (W, Ti)C_{1-x} has a primitive cell volume of 20.26 Å^3, 20.76 Å^3 and 18.99 Å^3, respectively. With respect to TiC phase, differences in primitive cell volumes are −6.27% for (W, Ti)C_{1-x} and +2.47% for WC. Fig. 5 shows a

Table 3. Errors in primitive cell volume calculation from Si [001] CBED pattern with three camera length values

	ZOLZ area error (%)	Error in HOLZ spacing (%)	Primitive cell volume error (%)
No correction (Eq. (7))	1.91	0.14	2.06
Geometrical correction (Eq. (8))	1.93	0.84	2.78
Least square fitting (Eq. (9))	0.18	23.02	23.25

core-shell microstructure in WC-TiC grain where inner TiC grain is surrounded by (W, Ti)C_{1-x} grain. Points of analysis for CBED and energy dispersive X-ray spectroscopy (EDXS) are numbered in the bright-field TEM image given in Fig. 5(a). Results are lists in Fig. 5(b) and plotted in Fig. 6.

DISCUSSION

1. Derivation of equations for real-time primitive cell volume measurements

Si [111] CBED pattern and measurement values are given in Fig. 1 for real-time measurement and film measurement from the identical pattern. Note that the values from real-time measurements have the unit of nm and are calculated automatically by incorporating the camera constant value. Therefore, accurate internal calibration of camera length has to be made in advance. This unit is conveniently used to compare the interplanar spacings of the phase being investigated. Equations for primitive cell volume measurement are modified accordingly and become much simpler as shown in Eq. (4)-(6). Typically, less than a minute is enough to measure the CBED pattern on the screen and calculate the primitive cell volume from the pattern. If calculated primitive cell volume matches to theoretical value from expected constituent phase, then the pattern is recorded on the film for film measurements. This approach for nano-phase materials is quite reliable since primitive cell volume from the nano-phase regions can be checked with theoretical values of constituent phases whether it is redundant or necessary and only necessary set of

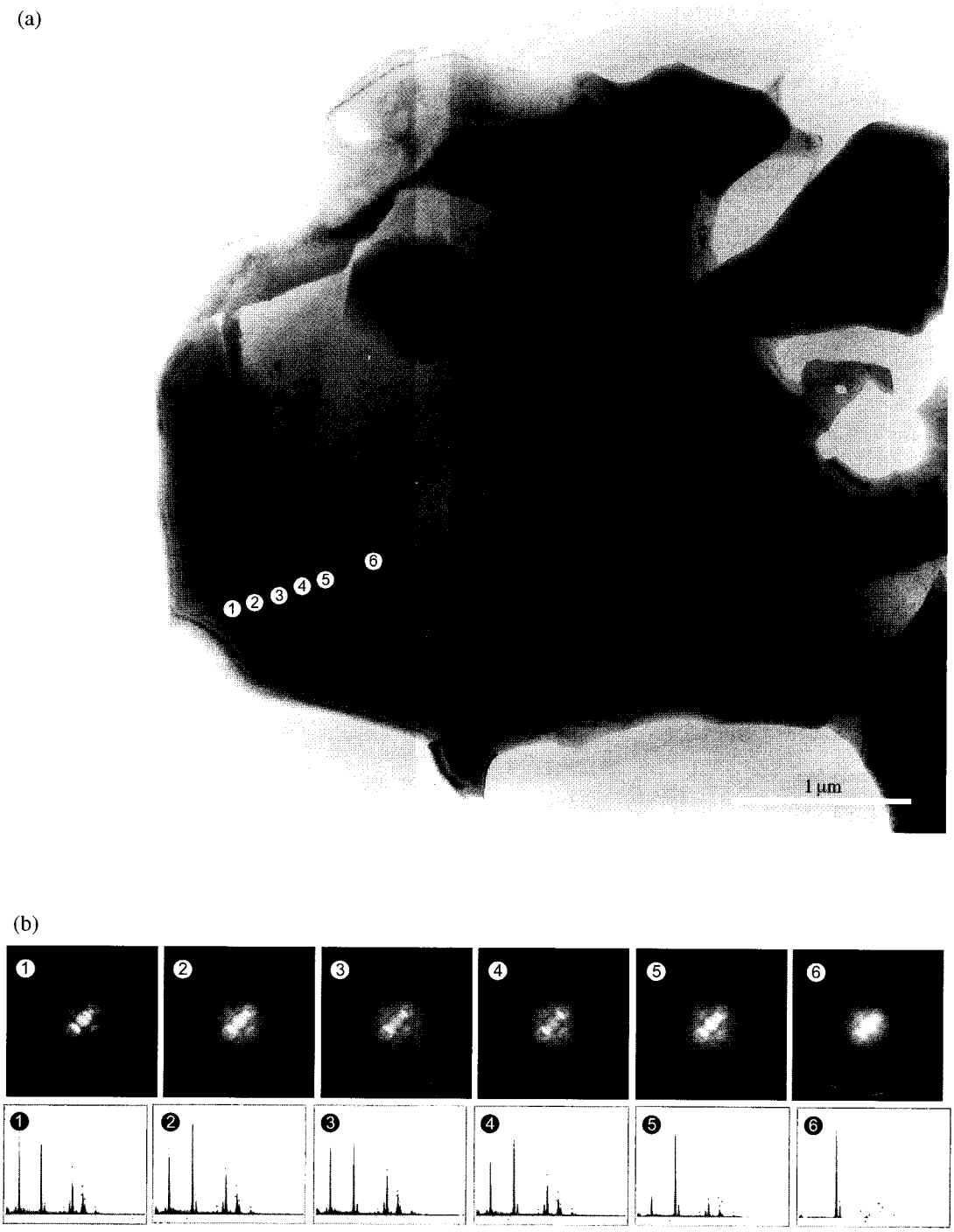

Fig. 5. TEM image of WC-TiC grains and points of analysis for CBED patterns and energy dispersive X-ray spectroscopy, (a) Bright field image of core-shell type grain and the point of analysis marked by numbers, (b) results of CBED patterns and EDXS spectra taken from the positions marked by numbers in (a).

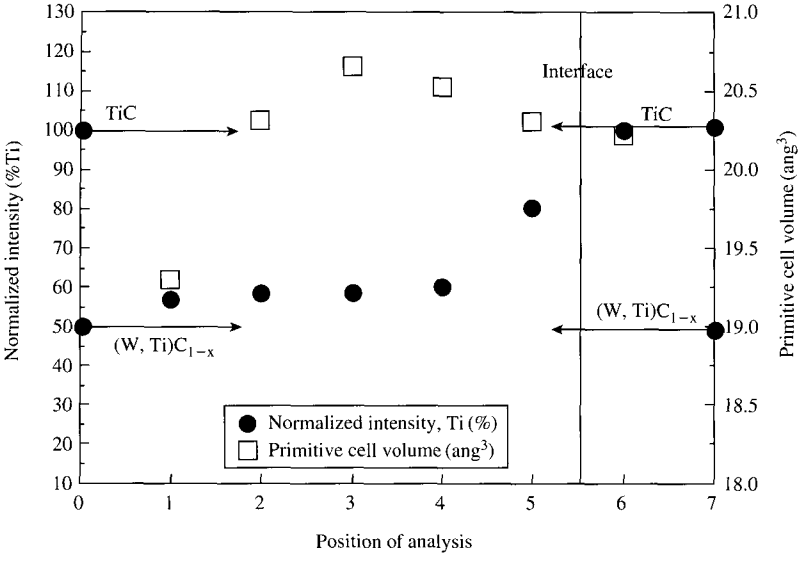

Fig. 6. Variation of measured primitive cell volumes and normalized concentration (wt%) of Ti as a function of positions of analysis marked in Fig. 5(a).

patterns can be recorded.

2. Comparison of accuracy for primitive cell volume measurements

Data obtained from ZOLZ patterns and HOLZ rings are used to estimate and compare the accuracy for primitive cell volume measurements from the film and real-time method. In both cases, large error is originated from HOLZ ring measurements. Measurement error from ZOLZ reflections is in the range of 2~3% while that of HOLZ ring radii is about 5~8%. Largest error is found in real-time measurement of the HOLZ rings. It is believed that the main source of error comes from the inaccuracy or non-linearity of camera length with respect to spot distances. At any rate, careful film measurement technique can lead to accuracy of up to 5% while in real-time measurement, accuracy of about 8% is estimated value for primitive cell volume measurements.

3. Phase identification in Mo-Si-N system

Molybdenum has an excellent high temperature strength and ductility and is regarded as a good refractory metal. However, poor oxidation resistance of Mo prevents its wide applications in high temperature structural components. One approach to improve the high temperature oxidation resistance is to create $MoSi_2$ coating layer on the surface by diffusion and reaction of Si. Short-term oxidation resistance is readily improved with this coating method, but during long exposure to high service temperature, silicon diffuses inward to form 3 intermetallic phases and eventually, $MoSi_2$ layer is consumed to form Mo_5Si_3 or Mo_3Si layer, which does not have a good protection against oxidation. Another potential problem of this monolithic coating is the formation of cracks in the coating layer during cooling from high temperature due to differences in thermal expansion coefficient with Mo substrate. To alleviate these problems in $MoSi_2$ coating layer on Mo substrate, in-situ formation of reinforcing nano particulates in $MoSi_2$ layer is attempted by two-step CVD process. Mo_2N surface layer is formed by nitriding the Mo_5Si_3 layer in the first stage and silicon is deposited to form $MoSi_2$ matrix and finely dispersed Si_3N_4 nano grains by diffusion and displacive reaction. Resulting microstructure consists of $MoSi_2$, Mo_3Si, Si_3N_4 and Mo_2N phase mixed in nanoscale. Identification of phase distribution in coating layer is not easy with conventional selected area electron diffraction technique due to small size of grains or with film measurement from CBED pattern since

phases have a similar morphology. Fortunately, four phases in this coating layer have quite different primitive cell volumes and real-time measurement with 10% accuracy can be employed satisfactorily in this case. Results listed in Table 2 and Fig. 2 clearly shows the advantage of using real-time technique for phase identification and with a minimum effort, all 4 phases constituting the coating layer are distinguished. It is worth noting that the accuracy of real-time method can be checked by analyzing the film afterwards and the results in Table 2 suggests that comparable accuracy is achieved in both methods.

4. Correction of errors in primitive cell volume measurements

Calibration of camera length is done by using the Si [001] CBED pattern shown in Fig. 3. Main reason to use this zone axis pattern is that 4-fold symmetry gives rise to 4 spots with identical distance for each type of reflection such as {220}, {400}, {440}, {800} and {660}. Scattering of 4 data points from each reflection gives information on measurement errors. In addition, large diffraction angles from high index reflections of ZOLZ spots such as {800} or {660} can be easily observed and calibrated values of such large diffraction angles can be directly applied to HOLZ ring measurements from low symmetry zone axis patterns. Data from Fig. 3 is plotted in Fig. 4 and three models for camera length are fitted with the data to understand the role of camera length on accuracy of primitive cell measurements. Simple linear relationship described in Eq. (7) does not have any correction term and by comparing with experimental data, it is evident that large error is inevitable for the calculation of interplanar spacing or primitive cell volumes. It overestimates the interplanar spacing at low diffraction angle and *vise versa*. Slightly improved model of camera length variation expressed in Eq. (8) has correct trend with experimental data but the slope is too small to compensate the errors coming from dependence of camera length with diffraction angle. Least square fitting approach in Eq. (9) shows much improved variation of camera constant with diffraction angle. Accuracies in ZOLZ area, HOLZ spacing and primitive cell volume calculation from aforementioned three cases are compared in Table 3. Interestingly, first two cases show comparable error values of about 3% for primitive cell volume measurements and main source of error is from ZOLZ area determination. On the other hand, least square fitting procedure yields smallest error in ZOLZ measurements as one may expect from Fig. 4. However, gross error is introduced in HOLZ spacing calculation exceeding the error of 23%. This is obviously unacceptable and clear explanation for this behavior is still pursued. One possible solution may be that different calibration curve has to be used separately for ZOLZ reflections and HOLZ rings. Since first two methods have a comparable error value of 5% including the standard deviation, no correction is used to for the analysis of WC-TiC grains.

5. Primitive cell volume measurements in WC-TiC core-shell structure

Variations in primitive cell volumes in WC-TiC grains are measured and combined with chemical compositional variation determined by EDXS method. Fig. 5 shows the image of core-shell structure and results of CBED patterns and EDXS spectra obtained from points marked by numbers in Fig. 5(a). Both grains have identical crystallographic orientation characteristic of core-shell structure. Surrounding grain of (W, Ti)C_{1-x} has dark contrast due to high content of W. Measured primitive cell volumes from CBED patterns and concentrations of Ti in wt% from normalized intensities of EDXS spectra are plotted in Fig. 6. Variation in cell volume at different positions of analysis is clearly shown and somewhat different variation of chemical composition by EDXS can be found. Primitive cell volume variation exhibits rapidly increasing trend as positions of analysis approaches the interface and becomes almost constant around the interface. Chemical compositional variation, on the other hand, shows slowly increasing variation of Ti contents up to the interface region. Plausible explanation for this behavior in Fig. 6 is that for primitive cell volume variation across the interface, lattice continuity exists and primitive cell volume should also have the continuity. But the compositional profile of Ti should vary abruptly as appeared in Fig. 6. Therefore primitive cell volume profile measured from CBED patterns of the core-shell structure reveals unique lattice dimensional variation and can provide additional information unavailable from chemical analysis. Another important point to note is that the HOLZ pattern analysis

to elucidate the lattice parameter variation may not be successful from the region close to the interface due to existing high strain. In fact, HOLZ pattern from (W, Ti)C_{1-x} grain is not observed near the interface (position ⑤ in Fig. 5(a)), but primitive cell volume is measured without any difficulty. One may be concerned about the accuracy of this method as compared to HOLZ pattern analysis for lattice parameter determination. It can be argued that the measurement of volume strain is much easier than measuring the linear strain. For example, if lattice parameter of silicon is changed from 0.543 nm to 0.544 nm, this change is causing the 0.18% linear strain or 0.5% of volume strain. Therefore, volume strain measurement does not require a stringent precision as in linear strain measurement. However, to be more quantitative method of structural characterization method, the accuracy of primitive cell volume measurement has to be improved up to 1 or 2% level and this requires careful calibration of camera length and reduction of measurement error from the CBED patterns.

In summary, real-time phase identification using a single CBED pattern has been investigated to apply this technique to nano-scale phase analysis, To achieve this goal, simplified equation for primitive cell volume calculation is derived and its accuracy is evaluated. Typical accuracy of 5% is confirmed and further improvement of accuracy is attempted with careful calibration of camera length. It is found that even with 5% accuracy, this technique is applicable to more complicated microstructures such as core-shell grains. Two examples of phase analysis are given to illustrate the reliability and accuracy of this method. In the first example, the phase analysis of nanocomposite coating with four constituent phases is done with real-time analysis. Core-shell grain found in the TiC-WC system is analyzed in the second example to get primitive cell volume variation in nano-scale and information on interfacial integrity or coherent strain can be obtained.

REFERENCES

Andrews KW, Dyson DJ, Keown SR: Interpretation of Electron Diffraction Patterns, Adam Hilger Ltd., Glasgow, pp. 20, 1971.

Byun JY, Yoon JK, Kim GH, Kim JS, Choi CS: Scripta Materialia 46 : 537, 2002.

Edington JW: Practical Electron Microscopy in Materials Science, TechBooks, Herndon, pp. 8, 1976.

Kim GH, Kim HS, Kum DW: Microscopy Research and Technique 33 : 510, 1996.

Page LY: Microscopy Research and Technique 21 : 158, 1992.

Pool Jr CP, Owens FJ: Introduction to Nanotechnology John Wiley & Sons, Inc., New Jersey, pp. 72, 2003.

Schamp CT, Jesser WA: Ultramicroscopy 103 : 165, 2005.

Yoon JK, Kim GH, Han JH, Shon IJ, Doh JM, Hong KT: Surface and Coatings Technology 7 : 2537, 2005.